

A Family of Kinematically Redundant Planar Parallel Manipulators

Iman Ebrahimi
Ph.D. Candidate
e-mail: iman.ebrahimi@unb.ca

Juan A. Carretero¹
Assoc. Professor
e-mail: juan.carretero@unb.ca

Department of Mechanical Engineering,
University of New Brunswick,
Fredericton, NB, E3A 5A3, Canada

Roger Boudreau
Professor
Département de Génie Mécanique,
Université de Moncton,
Moncton, NB, E1A 3E9, Canada
e-mail: roger.a.boudreau@umoncton.ca

Parallel manipulators feature relatively high payload and accuracy capabilities compared to their serial counterparts. However, they suffer from small workspace and low maneuverability. Kinematic redundancy for parallel manipulators can improve both of these characteristics. This paper presents a family of new kinematically redundant planar parallel manipulators with six actuated-joint degrees of freedom based on a 3-PRRR architecture obtained by adding an active prismatic joint at the base of each limb of the 3-RRR manipulator. First, the inverse displacement of the manipulators is explained, then their reachable and dexterous workspaces are obtained. Comparing the proposed redundant manipulators to the original 3-RRR nonredundant manipulator, both reachable and dexterous workspaces are substantially larger. Next, the Jacobian matrices of the manipulators are derived, and different types of singularities are analyzed and demonstrated. It is shown that the vast majority of singularities can be avoided by using kinematic redundancy. [DOI: 10.1115/1.2900723]

1 Introduction

Higher accuracy, speed, and payload-to-weight ratio are the major advantages of parallel manipulators compared to serial manipulators. A smaller workspace, reduced dexterity, as well as complex kinematic and dynamic models are their major drawbacks. Much research has been conducted on kinematics and dynamics of parallel manipulators [1–8], as well as on singularity and workspace analyses [9–13].

The vast majority of the studies on parallel manipulators have focused on nonredundant parallel manipulators. Redundant parallel manipulators have been introduced to alleviate some of the aforementioned shortcomings of parallel manipulators. Redundancy in parallel manipulators was introduced in Refs. [14–16]. Redundancy can be divided into two main types: actuation redundancy and kinematic redundancy. *Actuation redundancy* is defined as replacing existing passive joints of a manipulator by active ones. Actuation redundancy does not change the mobility or reachable workspace of a manipulator but entails the manipulator having more actuators than are needed for a given task and may be used to reduce the singularities within the manipulator's workspace [17]. For example, the planar 3-RRR² parallel manipulator, shown in Fig. 1, becomes redundantly actuated when a normally passive revolute joint such as B_i or D_i is replaced with an active joint.

Kinematic redundancy increases the mobility and actuated-joint degrees of freedom (ADOFs) of parallel manipulators. Kinematic redundancy takes place when extra active joints and links (if needed) are added to manipulators. For instance, by adding one extra active prismatic joint to one limb of the 3-RRR, it is converted into a kinematically redundant parallel manipulator (see Fig. 2). In this example, the resulting redundant parallel manipu-

lator has 4-ADOF, one more than the planar task space. In general, kinematic redundant parallel manipulators need more controlling parameters than required for a set of given tasks [17]. A manipulator with sufficient kinematic redundancy can avoid all interior singularities, has a larger workspace, and improved maneuverability [18]. Using kinematic redundancy can also allow manipulators to cope with joint-jam failure (e.g., Ref. [19]).

Compared to other research that has been pursued for parallel manipulators, redundancy in such manipulators has not adequately been studied. In serial manipulators, the concept of kinematic redundancy has been broadly studied (see, for instance, Refs. [20–22]).

In the present work, a family of 6-ADOF kinematically redundant planar parallel manipulators is introduced. Note that the task space of all the manipulators that are considered in this work is a three degrees of freedom planar motion. First, the proposed 3-PRRR manipulator family obtained by adding an active prismatic joint at the base of each limb of a 3-RRR manipulator is presented. Then, their inverse displacement problem (IDP) is explained. Thereafter, the reachable and dexterous workspaces of the original nonredundant 3-RRR manipulator are obtained and compared to those of the redundant manipulators. Finally, the direct, inverse, and combined singularities of the aforementioned manipulators are analyzed and illustrated.

2 Proposed Architectures

Adding one degree of kinematic redundancy (1-DOKR) can considerably reduce the number of direct kinematic singularities of a 3-RRR planar manipulator but not all of them [17]. By adding 2-DOKR, it is possible to avoid all direct kinematic singularities of the 3-RRR manipulators. A symmetrical architecture is usually desirable. Also, as is shown later, kinematic redundancy increases the workspace; hence, 1-DOKR is added here to each limb of the 3-RRR manipulator producing manipulators with a total of 3-DOKR. Therefore, the family of redundant manipulators proposed here has 6-ADOF for a planar task, three of which are redundant. The added kinematic redundancies enable the manipulators to avoid kinematic singularities, improve their maneuverability, and enlarge their reachable and dexterous workspaces.

Figures 3–5 illustrate a new family of three 6-ADOF redundant planar parallel manipulators. The notation used for each manipulator is based on the shape of the guides on which the redundant

¹Corresponding author.

²The terminology used is the following. A 3-RRR mechanism indicates that the end effector is connected to the base by three serial kinematic chains (limbs), each consisting of an active (and therefore underlined) revolute joint (R) connected to the base, followed by two passive revolute joints, the second of which connects the limb to the end effector. In the adopted notation, a prismatic joint would be shown by a P and would be underlined if it were active.

Contributed by the Mechanisms and Robotics Committee of ASME for publication in the JOURNAL OF MECHANICAL DESIGN. Manuscript received February 13, 2007; final manuscript received October 5, 2007; published online April 15, 2008. Review conducted by Pierre M. Laroche, P.E.

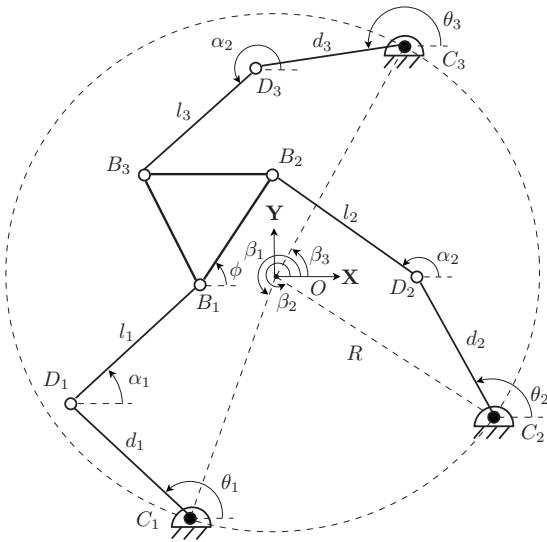


Fig. 1 3-RRR planar parallel manipulator

prismatic actuators slide. All 3-PRRR manipulators are based on the nonredundant 3-RRR planar parallel manipulator proposed in Ref. [23] (Fig. 1). Each limb of the 3-PRRR manipulators has one prismatic actuator at its base. Adding prismatic redundant actuators close to the base causes less dynamic effects due to the weight of the actuators.

The redundant prismatic actuators slide on their respective guides that can take the shape of a triangle, a star, and a circle. The notation is thus 3-PRRR Δ , 3-PRRR \star , and 3-PRRR \circ for guides that have a triangle, star, or circle shape, respectively. Note that the 3-PRRR \circ manipulator is, in fact, a 3-RRRR manipulator, since a circular prismatic joint with a finite radius is, in fact, a revolute joint. The 3-PRRR \circ notation is maintained to more readily identify the similarities of each manipulator in the proposed family. An actuated revolute joint is mounted on the prismatic actuator at Point A_i (throughout the present work, $i = 1, 2, 3$). Note that the solid circles in all the figures represent active revolute joints, whereas the empty circles represent passive ones. Finally, two passive revolute joints are at D_i and B_i , where Point B_i is attached to the end effector.

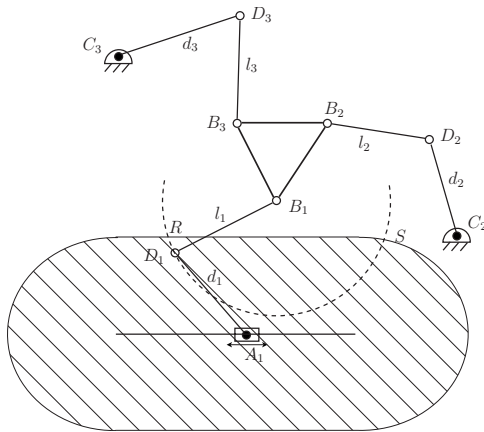


Fig. 2 4DOF kinematically redundant planar parallel manipulator and its locus of solutions for the IDP, shown as arc $\widehat{RD_1S}$

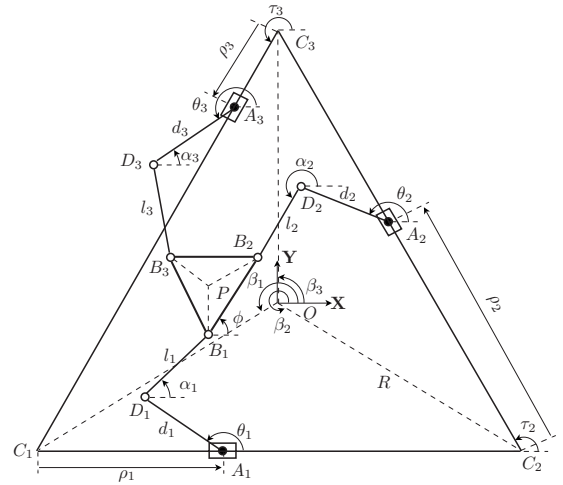


Fig. 3 3-PRRR Δ planar 6-DOF kinematically redundant parallel manipulator

3 Inverse Displacement of the Proposed Architectures

Kinematic redundancy in manipulators results in having an infinite number of solutions to the IDP. That is, rather than having a finite number of solutions, there may be one or more loci of joint variable values (angles or lengths) for a given position and orientation of the end effector. Figure 2 illustrates a situation where, by adding an extra prismatic actuator to the first limb, 1-DOKR is added to that limb of a 3-RRR planar parallel manipulator. The resulting kinematically redundant manipulator has 4-ADOF for a planar task. That is, as long as two circles centered at B_1 and A_1 and radii of l_1 and d_1 , respectively, intersect each other, there are infinite solutions for the IDP of the manipulator.

The hatched region in Fig. 2 shows the area that Point D_1 of Link A_1D_1 can cover when the prismatic Actuator A_1 slides within a certain range and Link A_1D_1 rotates around Point A_1 . As it is evident from Fig. 2, Point D_1 as a part of Link B_1D_1 (pinned at Point B_1) can rotate a full circle around Point B_1 . Therefore, all possible solutions of the IDP for that limb lie on the intersection of the aforesaid regions. Assuming that the IDP exists for Limb 1, the redundant manipulator has a locus of solutions shown as arc $\widehat{RD_1S}$. Note that the IDP for each limb of the original nonredundant 3-RRR has at the most two solutions.

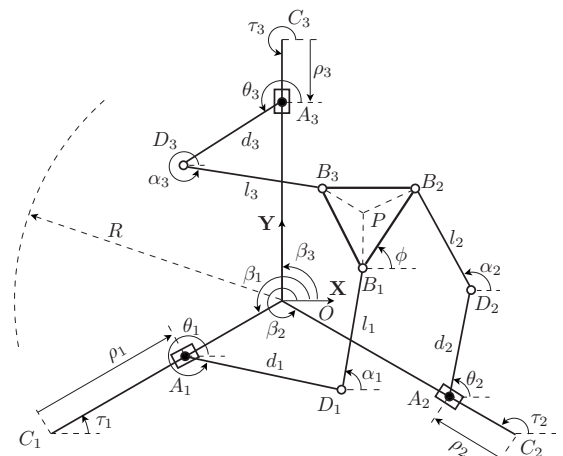


Fig. 4 3-PRRR \star planar 6-DOF kinematically redundant parallel manipulator

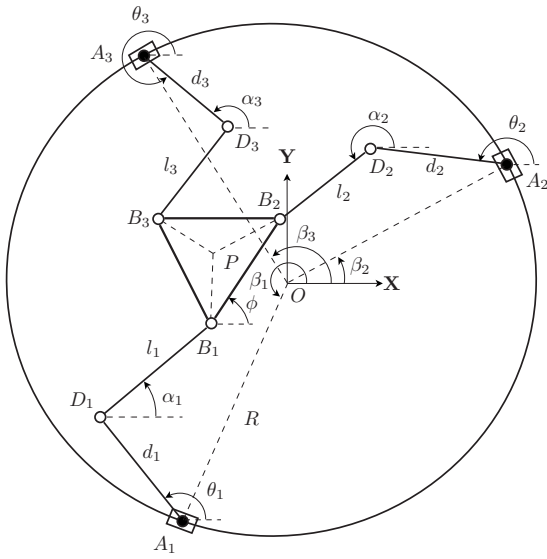


Fig. 5 3-PRRR_O planar 6-ADOF kinematically redundant parallel manipulator

Finding the best inverse displacement solution for redundant manipulators is normally formulated as a numerical optimization problem [21]. To find an optimal solution of the IDP, different cost functions may be defined for different purposes such as minimum energy, distance, time, or condition number [21,24]. Note that once a position for one of the active Joints A_i or θ_i is chosen, there are only two solutions for the IDP for each limb for a given position and orientation of the end effector.

Figure 6 shows the details of the end effector and its associated dimensions, which are the same for all the manipulators. Considering that the end-effector location is measured from Point P and the geometry, of the 3-PRRR manipulator family as shown in Figs. 3–6, the IDP of the manipulator can be written as

$$\overline{D_i B_i} = \overline{D_i A_i} + \overline{A_i O} + \overline{OP} + \overline{PB_i} \quad (1)$$

Equation (1) can be expressed as

$$x_{D_i B_i}^2 + y_{D_i B_i}^2 = x_{(D_i A_i + A_i O + OP + PB_i)}^2 + y_{(D_i A_i + A_i O + OP + PB_i)}^2 \quad (2)$$

$$x_{D_i B_i}^2 + y_{D_i B_i}^2 = l_i^2 \quad (3)$$

For the 3-PRRR_Δ and the 3-PRRR_★ manipulators, the inverse displacement equations can be written as

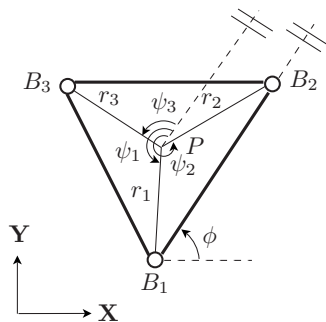


Fig. 6 End-effector details for all the manipulators

$$l_i^2 = (x_p + r_i c_{(\phi + \psi_i)} - R c_{\beta_i} - \rho_i c_{\tau_{i\Delta, \star}} - d_i c_{\theta_i})^2 + (y_p + r_i s_{(\phi + \psi_i)} - R s_{\beta_i} - \rho_i s_{\tau_{i\Delta, \star}} - d_i s_{\theta_i})^2 \quad (4)$$

where c_{\angle} and s_{\angle} represent $\cos(\angle)$ and $\sin(\angle)$, respectively. All angles except ψ_i (which is measured relative to $B_1 B_2$, see Fig. 6) are measured with respect to the X-axis. Also, a double architecture identification symbol indicates the angle to be used depending on the considered kinematic architecture. For example $c_{\tau_{3\Delta, \star}}$ refers to the cosine of $\tau_{3\Delta}$ or $\tau_{3\star}$ depending on the architecture. Angles τ_i are defined as

$$\begin{aligned} \tau_{1\Delta} &= 0 & \tau_{1\star} &= \frac{\beta_1 - \beta_2 + \pi}{2} \\ \tau_{2\Delta} &= \frac{\beta_3 - \beta_1 + 2\pi}{2} & \tau_{2\star} &= \frac{\beta_2 - \beta_1 + \pi}{2} \\ \tau_{3\Delta} &= \frac{\beta_3 - \beta_2 + 4\pi}{2} & \tau_{3\star} &= \frac{2\beta_3 - \beta_2 - \beta_1 + \pi}{2} \end{aligned} \quad (5)$$

Similarly, for the 3-PRRR_O manipulator, the inverse displacement equations can be written as

$$l_i^2 = (x_p + r_i c_{(\phi + \psi_i)} - R c_{\beta_i} - d_i c_{\theta_i})^2 + (y_p + r_i s_{(\phi + \psi_i)} - R s_{\beta_i} - d_i s_{\theta_i})^2 \quad (6)$$

For the 3-PRRR_Δ and 3-PRRR_★ manipulators, the end effector pose and the actuator vectors can be expressed as $\mathbf{x} = [x_p, y_p, \phi]^T$ and $\mathbf{q} = [\rho_1, \theta_1, \rho_2, \theta_2, \rho_3, \theta_3]^T$, respectively. For the 3-PRRR_O manipulator, they can be defined as $\mathbf{x} = [x_p, y_p, \phi]^T$ and $\mathbf{q} = [\beta_1, \theta_1, \beta_2, \theta_2, \beta_3, \theta_3]^T$, respectively.

Regardless of the optimization method that is chosen, the selected inverse displacement solution depends on the initial pose and configuration of each limb as well as the cost function that is used [18,24]. This work mainly focuses on introducing a family of kinematically redundant planar manipulators and analyzing the manipulators' workspace and kinematic singularities. Optimal path selection is an extensive topic on its own and is left for subsequent research.

4 Workspace Comparison of the Manipulators

In this work, two types of workspaces are studied: reachable and dexterous. The reachable (maximal) workspace is considered here as the region that contains every point that can be reached by the end effector in at least one orientation [25]. The condition for being accepted as a point in the reachable workspace is the existence of a solution to the IDP while considering only the position of the end effector. The dexterous workspace, on the other hand, is considered as the region of the reachable workspace that can be reached by the end effector with all possible orientations (from zero to 2π) [25]. The dexterous workspace of each of the four manipulators analyzed here is geometrically obtained, as shown in Figs. 7(b), 8(b), 9(b), and 10(b), for the 3-RRR, 3-PRRR_Δ, 3-PRRR_★, and 3-PRRR_O, respectively. For every branch of any of the 3-PRRR manipulators, each leg can slide at Point A_i . The dexterous workspace of each branch can be represented by a circle whose radius is $l_i + d_i - r_i$ and is swept along slider i . The intersection of the three regions made by the reachable workspace of the three branches will be the dexterous workspaces of the manipulator [26]. For the 3-RRR, the same process is followed except that the circle representing the reachable workspace of each branch is kept with its center at a constant location C_i .

The reachable workspaces of the manipulators can be geometrically obtained too but, due to the complexity and lengthiness of the procedure, it is not explained here. For details, one can refer to the work that was done in Ref. [26] for the nonredundant 3-RPR.

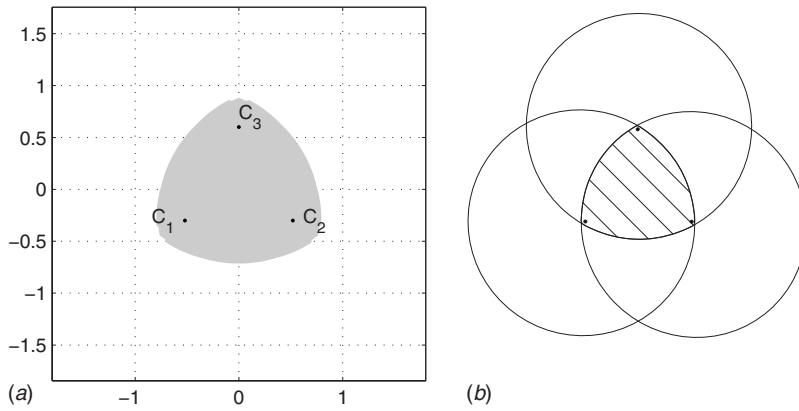


Fig. 7 Workspaces of the 3-RRR nonredundant planar parallel manipulator

Here, the reachable workspace of each of the manipulators is numerically obtained and will be used for comparing the manipulators' capabilities.

The reachable and dexterous workspaces of the 3-RRR nonredundant manipulator are shown in Fig. 7. The workspaces of the redundant 3-PRRR manipulators are compared in Figs. 8–10. In Figs. 8–10, the base platforms (the sliders' guides) are identified as the triangle $C_1C_2C_3$, the star $C_1C_2C_3$, and the circle, respectively. The geometric parameters for the 3-RRR and all the 3-PRRR manipulators analyzed here are $R=0.6$ m, $l_i=0.6$ m, $d_i=0.6$ m, $r_i=0.1155$ m, $\psi_1=7\pi/6$, $\psi_2=11\pi/6$, $\psi_3=\pi/2$, and $\sphericalangle C_1OC_2=\sphericalangle C_1OC_3=2\pi/3$.

Table 1 shows the absolute and relative sizes (written as Abs. and Rel., respectively) of the reachable and dexterous workspaces of the 3-PRRR manipulators relative to 3-RRR. As expected, both the reachable and dexterous workspaces of the 3-PRRR manipulators are considerably larger than those of the 3-RRR manipulator.

Considering the last column of Table 1, it can also be inferred that kinematic redundancy results in considerable increase in the ratio of the dexterous over the reachable workspace area compared to the nonredundant 3-RRR manipulator. This ratio varies for the different arrangements of the prismatic redundant actuators.

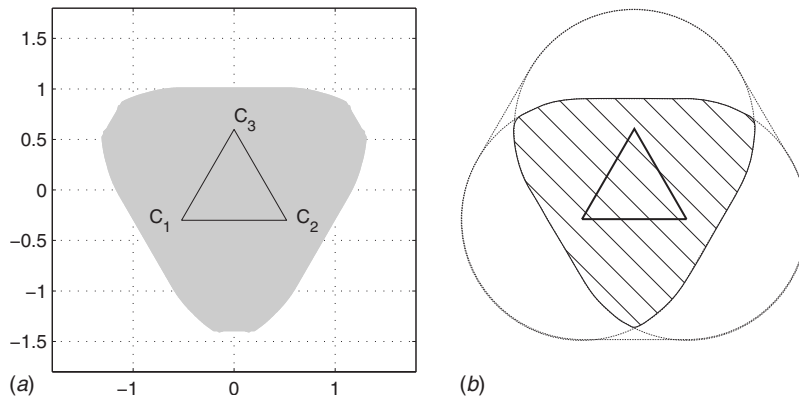


Fig. 8 Workspaces of the 3-PRRR $_{\Delta}$ redundant planar parallel manipulator

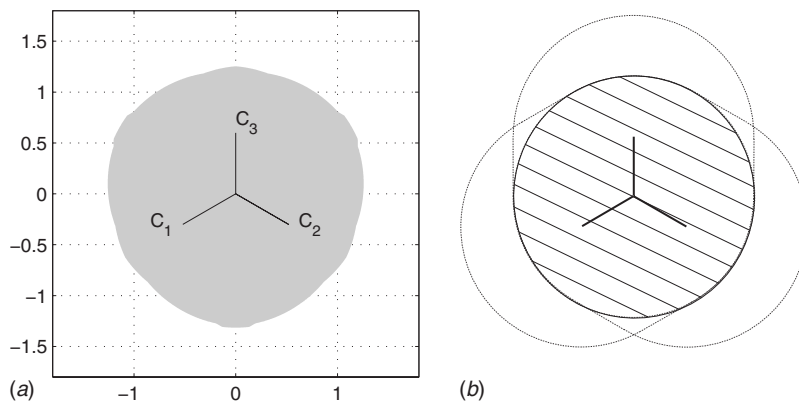


Fig. 9 Workspaces of the 3-PRRR $_{*}$ redundant planar parallel manipulator

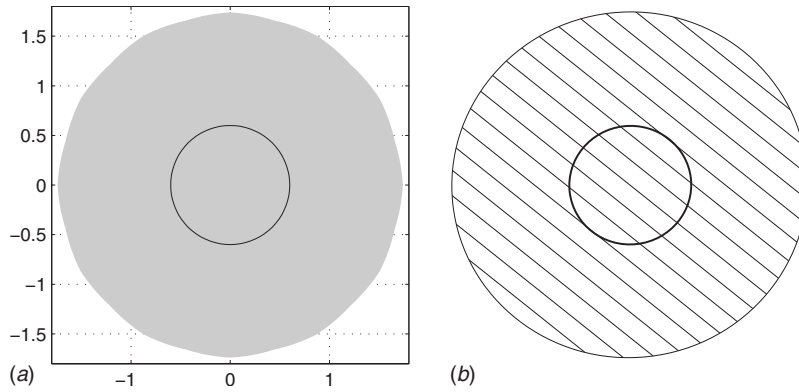


Fig. 10 Workspaces of the 3-PRRR_O redundant planar parallel manipulator

tors, with the maximum value being for the circular prismatic redundant actuators and the minimum for the triangle-shape path.

5 Kinematic Singularity Analysis

5.1 Types of Kinematic Singularities. Jacobian matrices transform the velocity vector of the end effector into a velocity vector of the active joints. That is,

$$\mathbf{J}_x \dot{\mathbf{x}} = \mathbf{J}_q \dot{\mathbf{q}} \quad (7)$$

where $\dot{\mathbf{x}}$ is the velocity vector of the end effector $\dot{\mathbf{x}} = [\dot{x}_p, \dot{y}_p, \dot{\phi}]^T$, and $\dot{\mathbf{q}}$ is the velocity vector of the associated active joints, $\dot{\mathbf{q}} = [\dot{\rho}_1, \dot{\theta}_1, \dot{\rho}_2, \dot{\theta}_2, \dot{\rho}_3, \dot{\theta}_3]^T$ for the 3-PRRR_Δ and 3-PRRR_★ manipulators and $\dot{\mathbf{q}} = [\dot{\beta}_1, \dot{\theta}_1, \dot{\beta}_2, \dot{\theta}_2, \dot{\beta}_3, \dot{\theta}_3]^T$ for the 3-PRRR_O manipulator. Considering Eq. (7), three types of kinematic singularities can be defined for parallel manipulators [27].

1. Direct kinematic singularities when \mathbf{J}_x is singular.
2. Inverse kinematic singularities when \mathbf{J}_q is singular.
3. Combined (complex) singularities when \mathbf{J}_x and \mathbf{J}_q are singular.

Direct kinematic singularities (i.e., $|\mathbf{J}_x| = 0$) take place when there are some nonzero velocities of the end effector that are possible with zero velocities at the actuators. Also, direct kinematic singularities are referred to as force uncertainties or as force unconstrained poses [28]. On the other hand, inverse kinematic singularities (i.e., when $|\mathbf{J}_q| = 0$) happen when there exist some nonzero actuator velocities that cause zero velocities for the end effector. In order to perform a kinematic singularity analysis on the introduced 3-PRRR manipulator family, their Jacobian matrices are obtained in the following section.

5.2 Jacobian Matrices of the 3-PRRR Manipulators. By differentiating Eq. (4) with respect to time, the Jacobian matrices are given by

$$\mathbf{J}_{x_{\forall}} = \begin{bmatrix} t_{11_{\forall}} & t_{12_{\forall}} & t_{13_{\forall}} \\ t_{21_{\forall}} & t_{22_{\forall}} & t_{23_{\forall}} \\ t_{31_{\forall}} & t_{31_{\forall}} & t_{33_{\forall}} \end{bmatrix}_{3 \times 3} \quad (8)$$

$$\mathbf{J}_{q_{\forall}} = \begin{bmatrix} u_{1_{\forall}} & v_{1_{\forall}} & 0 & 0 & 0 & 0 \\ 0 & 0 & u_{2_{\forall}} & v_{2_{\forall}} & 0 & 0 \\ 0 & 0 & 0 & 0 & u_{3_{\forall}} & v_{3_{\forall}} \end{bmatrix}_{3 \times 6} \quad (9)$$

where $\forall = \Delta, \star, \circ$, depending on the manipulator. For the 3-PRRR_Δ and 3-PRRR_★ manipulators, the elements are

$$t_{i1_{\Delta, \star}} = x_p + r_i c_{(\phi + \psi_i)} - R c \beta_i - \rho_i c \tau_{i_{\Delta, \star}} - d_i c \theta_i \quad (10)$$

$$t_{i2_{\Delta, \star}} = y_p + r_i s_{(\phi + \psi_i)} - R s \beta_i - \rho_i s \tau_{i_{\Delta, \star}} - d_i s \theta_i \quad (11)$$

$$t_{i3_{\Delta, \star}} = -r_i s_{(\phi + \psi_i)} t_{i1_{\Delta, \star}} + r_i c_{(\phi + \psi_i)} t_{i2_{\Delta, \star}} \quad (12)$$

$$u_{i_{\Delta, \star}} = c_{\tau_{i_{\Delta, \star}}} t_{i1_{\Delta, \star}} + s_{\tau_{i_{\Delta, \star}}} t_{i2_{\Delta, \star}} \quad (13)$$

$$v_{i_{\Delta, \star}} = -d_i s_{\theta_i} t_{i1_{\Delta, \star}} + d_i c_{\theta_i} t_{i2_{\Delta, \star}} \quad (14)$$

whereas for the 3-PRRR_O, the elements are

$$t_{i1_{\circ}} = x_p + r_i c_{(\phi + \psi_i)} - R c \beta_i - d_i c \theta_i \quad (15)$$

$$t_{i2_{\circ}} = y_p + r_i s_{(\phi + \psi_i)} - R s \beta_i - d_i s \theta_i \quad (16)$$

$$t_{i3_{\circ}} = -r_i s_{(\phi + \psi_i)} t_{i1_{\circ}} + r_i c_{(\phi + \psi_i)} t_{i2_{\circ}} \quad (17)$$

$$u_{i_{\circ}} = -R s \beta_i t_{i1_{\circ}} + R c \beta_i t_{i2_{\circ}} \quad (18)$$

$$v_{i_{\circ}} = -d_i s_{\theta_i} t_{i1_{\circ}} + d_i c_{\theta_i} t_{i2_{\circ}} \quad (19)$$

Table 1 Workspace comparison for the nonredundant and redundant manipulators. All absolute quantities are in m².

	Reachable		Dexterous		Ratio Dexterous Reachable
	Abs.	Rel.	Abs.	Rel.	
3-RRR	1.89	1	0.92	1	0.49
3-PRRR _Δ	4.54	2.40	2.90	3.15	0.64
3-PRRR _★	5.00	2.64	3.70	4.02	0.74
3-PRRR _O	9.37	4.96	8.93	9.71	0.95

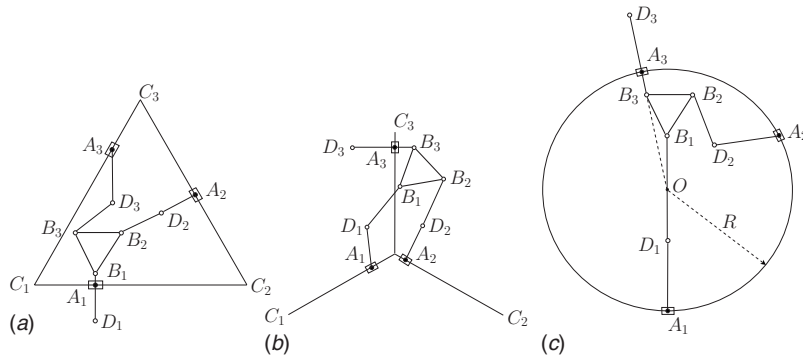


Fig. 11 Examples of the geometrical interpretations of the inverse kinematic singularities for the 3-PRRR manipulators

5.3 Direct Kinematic Singularities of the 3-PRRR Manipulators. The direct kinematic singularities of planar parallel manipulators with architectures whose distal links have passive revolute joints at both ends are the same. They all take place when the lines defining the distal links meet at a common point. The reason for this is that forces can only be transmitted in the distal link directions, and when all of them meet at a common point, the end effector can infinitesimally rotate around that point while all the actuators are locked. As shown in Figs. 3–5, all manipulators have passive revolute joints at both ends of the distal links (i.e., B_i and D_i).

The direct Jacobian matrix of all manipulators can be rewritten as

$$\mathbf{J}_{\mathbf{x}_v} = \begin{bmatrix} x_{l_1} & y_{l_1} & -r_1 s(\phi+\psi_1)x_{l_1} + r_1 c(\phi+\psi_1)y_{l_1} \\ x_{l_2} & y_{l_2} & -r_2 s(\phi+\psi_2)x_{l_2} + r_2 c(\phi+\psi_2)y_{l_2} \\ x_{l_3} & y_{l_3} & -r_3 s(\phi+\psi_3)x_{l_3} + r_3 c(\phi+\psi_3)y_{l_3} \end{bmatrix}_{3 \times 3} \quad (20)$$

$$= \begin{bmatrix} l_1 c_{\alpha_1} & l_1 s_{\alpha_1} & r_1 l_1 s(\alpha_1 - \phi - \psi_1) \\ l_2 c_{\alpha_2} & l_2 s_{\alpha_2} & r_2 l_2 s(\alpha_2 - \phi - \psi_2) \\ l_3 c_{\alpha_3} & l_3 s_{\alpha_3} & r_3 l_3 s(\alpha_3 - \phi - \psi_3) \end{bmatrix}_{3 \times 3}$$

where x_{l_i} and y_{l_i} are the projections of Links $B_i D_i$ onto the X and Y axes, respectively. The determinant of $\mathbf{J}_{\mathbf{x}_v}$ is zero, when there are linear dependencies between any two or more rows or columns. That is,

$$\lambda_1 \mathcal{W}_1 + \lambda_2 \mathcal{W}_2 + \lambda_3 \mathcal{W}_3 = 0 \quad (21)$$

where λ_i are scalar coefficients of linear dependency of which only up to two can be simultaneously zero and vector \mathcal{W}_i represents the i th row (or column) of $\mathbf{J}_{\mathbf{x}_v}$. Having only one λ_i nonzero represents configurations where all the elements of a row or a column are zero. Considering Eq. (20), the elements of the first or second column are zero when $x_{l_i} = 0$ or $y_{l_i} = 0$, respectively. These two conditions occur when all the distal links are parallel to the Y -axis or X -axis, respectively. In both cases, the distal links meet at a common point at infinity. The third column becomes zero, when all the distal links meet at Point P . Also, linear dependency between the rows have the same meaning as columns. Linear dependency between any two rows happens when two distal links are aligned with the side of the end effector that is between them.

Note that kinematic singularities are independent of the coordinate system. For the discussed manipulators, a singularity configuration only depends on relative positions and orientations of the distal links. Therefore, the aforementioned direct kinematic singularities can take place when all the distal links are parallel

regardless of the common direction or where they all meet at a common point.

5.4 Inverse Kinematic Singularities of the 3-PRRR Manipulators. For redundant parallel manipulators, the matrix $\mathbf{J}_{\mathbf{q}_v}$ is not square, and therefore, the inverse kinematic singularities can be said to occur when the rank of $\mathbf{J}_{\mathbf{q}_v}$ is lower than the degrees of freedom of the end effector [16], that is, the number of rows of $\mathbf{J}_{\mathbf{q}_v}$. Therefore, a kinematically redundant parallel manipulator is in an inverse kinematic singular configuration when any minor square matrix extracted from $\mathbf{J}_{\mathbf{q}_v}$ is singular. This degeneracy can also be identified as the condition that sets the determinant of $\mathbf{J}_{\mathbf{q}_v} \mathbf{J}_{\mathbf{q}_v}^T$ to zero. For the family of manipulators being presented,

$$\mathbf{J}_{\mathbf{q}_v} \mathbf{J}_{\mathbf{q}_v}^T = \begin{bmatrix} u_1^2 + v_1^2 & 0 & 0 \\ 0 & u_2^2 + v_2^2 & 0 \\ 0 & 0 & u_3^2 + v_3^2 \end{bmatrix}_{3 \times 3} \quad (22)$$

The elements of the matrix in Eq. (22) for the 3-PRRR $_{\Delta}$ and the 3-PRRR $_{\star}$ can be expressed as

$$u_{i_{\Delta, \star}} = l_i c(\alpha_i - \tau_i), \quad v_{i_{\Delta, \star}} = d_i l_i s(\alpha_i - \theta_i) \quad (23)$$

whereas those for the 3-PRRR $_{\circ}$ can be expressed as

$$u_{i_{\circ}} = R l_i s(\alpha_i - \beta_i), \quad v_{i_{\circ}} = d_i l_i s(\alpha_i - \theta_i) \quad (24)$$

Since matrix $\mathbf{J}_{\mathbf{q}_v} \mathbf{J}_{\mathbf{q}_v}^T$ is diagonal, its determinant becomes zero when any one or more of the diagonal elements become zero, that is, $u_{i_{\Delta, \star}}^2$ and $v_{i_{\Delta, \star}}^2$ would have to be simultaneously zero. For the 3-PRRR $_{\Delta}$ and the 3-PRRR $_{\star}$ manipulators, each diagonal element would be zero when both of the following conditions are satisfied:

$$\alpha_{i_{\Delta, \star}} = \frac{2n_1 + 1}{2} \pi + \tau_{i_{\Delta, \star}}, \quad n_1 = 0, 1, 2, \dots \text{ and} \quad (25)$$

$$\alpha_{i_{\Delta, \star}} = n_2 \pi + \theta_{i_{\Delta, \star}}, \quad n_2 = 0, 1, 2, \dots$$

The above conditions show that inverse kinematic singularities for the 3-PRRR $_{\Delta}$ and 3-PRRR $_{\star}$ manipulators occur when the sliding paths of the prismatic actuators (i.e., $C_i C_{i+1}$ for the 3-PRRR $_{\Delta}$ and $C_i O$ for the 3-PRRR $_{\star}$ manipulators) are perpendicular to $B_i D_i$ and also limb $A_i D_i B_i$ is fully stretched or fully folded (i.e., $A_i D_i \parallel D_i B_i$), as shown in Figs. 11(a) and 11(b).

For the 3-PRRR $_{\circ}$ manipulator, each diagonal element of $\mathbf{J}_{\mathbf{q}_v} \mathbf{J}_{\mathbf{q}_v}^T$ becomes zero when both of the following conditions are satisfied.

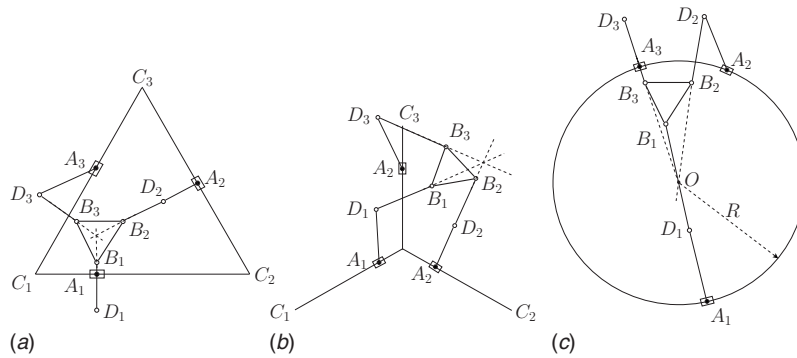


Fig. 12 Examples of the geometrical interpretations of the combined kinematic singularities for the 3-PRRR manipulators

$$\alpha_{i_O} = n_1\pi + \beta_{i_O}, \quad n_1 = 0, 1, 2, \dots \text{ and} \quad (26)$$

$$\alpha_{i_O} = n_2\pi + \theta_{i_O}, \quad n_2 = 0, 1, 2, \dots$$

The above conditions for the inverse kinematic singularities of the 3-PRRR_O imply that the inverse kinematic singularities take place when at least one limb is fully stretched or fully folded and also passes through the center of the circle (i.e., Point *O*). Figure 11(c) illustrates an inverse kinematic singular configuration when the first and third limbs are fully stretched and fully folded, respectively, and also pass through the center of the guide's circle for the prismatic actuators. It should be noted that for the entire family of 3-PRRR manipulators, as long as the manipulator is not in its workspace boundary, it is possible to choose one or more sets of joint displacements that avoid the inverse kinematic singularity conditions outlined here.

5.5 Combined (Complex) Kinematic Singularities of the 3-PRRR Manipulators. The combined kinematic singularities happen when both direct and inverse kinematic singularities take place; in other words, when both \mathbf{J}_{x_v} and $\mathbf{J}_{q_v}\mathbf{J}_{q_v}^T$ are singular. Figures 12(a)–12(c) show sample configurations in which both the direct and inverse singularities occur at the same time for the three manipulators of the 3-PRRR family introduced here.

6 Conclusions

A family of kinematically redundant planar parallel manipulators was proposed. Their IDPs were explained. Then, their reachable and dexterous workspaces were determined and compared to those of a similar-sized nonredundant manipulator. It was shown and compared that the novel manipulators have substantially larger reachable and dexterous workspaces. Thereafter, the kinematic singularity analyses were presented and their geometrical interpretations were explained for the 3-PRRR manipulator family. It can be generally concluded that inverse kinematic singularities occur for the whole family of 3-PRRR manipulators when at least one limb is fully stretched or fully folded while the limb is perpendicular to the sliding direction of the prismatic actuator, i.e., when the entire limb is collinear with the line that passes through the center of curvature of the slider's path at that point.

Generally, the proposed manipulators have loci of solutions for every pose inside their workspaces. Therefore, they have the capability to be programmed to optimize different cost functions such as minimum time and energy, while constrained to avoid kinematic singularities. The path shape of the prismatic redundant actuators (e.g., triangle, star, and circle) has a significant effect on the workspace shape. It was shown that kinematic redundancy not only increases the workspace of the manipulators but also significantly adds to the ratio of the dexterous workspace over the reachable workspace.

Acknowledgment

The authors would like to thank the Natural Sciences and Engineering Research Council of Canada (NSERC) for its support in funding this research.

References

- [1] Mohamed, M. G., and Duffy, J., 1985, "Direct Determination of the Instantaneous Kinematics of Fully Parallel Robot Manipulators," *ASME J. Mech., Transm., Autom. Des.*, **107**(2), pp. 226–229.
- [2] Yoshikawa, T., 1985, "Manipulability of Robot Mechanisms," *Int. J. Robot. Res.*, **4**(2), pp. 3–9.
- [3] Merlet, J.-P., 1993, "Direct Kinematics of Parallel Manipulators," *IEEE Trans. Rob. Autom.*, **9**(6), pp. 842–846.
- [4] Tahmasebi, F., and Tsai, L.-W., 1994, "Closed-Form Direct Kinematics Solution of a New Parallel Minimanipulator," *ASME J. Mech. Des.*, **116**(4), pp. 1141–1147.
- [5] Zanganeh, K., and Angeles, J., 1995, "Instantaneous Kinematics of General Hybrid Parallel Manipulators," *ASME J. Mech. Des.*, **117**(4), pp. 581–588.
- [6] Gosselin, C. M., 1996, "Parallel Computational Algorithms for the Kinematics and Dynamics of Planar and Spatial Parallel Manipulators," *ASME J. Dyn. Syst., Meas., Control*, **118**, pp. 22–28.
- [7] Boudreau, R., and Turkkan, N., 1996, "Solving the Forward Kinematics of Parallel Manipulators With a Genetic Algorithm," *J. Rob. Syst.*, **13**(2), pp. 111–125.
- [8] Nenchev, D. N., Bhattacharya, S., and Uchiyama, M., 1997, "Dynamic Analysis of Parallel Manipulators Under the Singularity-Consistent Parametrization," *Robotica*, **15**, pp. 375–384.
- [9] Sefrioui, J., and Gosselin, C. M., 1992, "Singularity Analysis and Representation of Planar Parallel Manipulators," *Rob. Auton. Syst.*, **10**(4), pp. 209–224.
- [10] Merlet, J.-P., 1995, "Designing a Parallel Manipulator for a Specific Workspace," Institut National de Recherche en Informatique et en Automatique, Technical Report No. 2527.
- [11] Innocenti, C., and Parenti-Castelli, V., 1998, "Singularity-Free Evolution From One Configuration to Another in Serial and Fully-Parallel Manipulators," *ASME J. Mech. Des.*, **120**(1), pp. 73–79.
- [12] Lee, M. K., and Park, K. W., 2000, "Workspace and Singularity Analysis of a Double Parallel Manipulator," *IEEE/ASME Trans. Mechatron.*, **5**(4), pp. 367–375.
- [13] Bonev, I. A., Zlatanov, D., and Gosselin, C. M., 2003, "Singularity Analysis of 3-DOF Planar Parallel Mechanisms via Screw Theory," *ASME J. Mech. Des.*, **125**(3), pp. 573–581.
- [14] Lee, S., and Kim, S., 1993, "Kinematic Analysis of Generalized Parallel Manipulator Systems," *Proceedings of the IEEE Conference on Decision and Control*, Vol. 2, pp. 1097–1102.
- [15] Zanganeh, K. E., and Angeles, J., 1994, "Instantaneous Kinematics and Design of a Novel Redundant Parallel Manipulator," *Proceedings of the IEEE Conference on Robotics and Automation*, San Diego, pp. 3043–3048.
- [16] Merlet, J.-P., 1996, "Redundant Parallel Manipulators," *Journal of Laboratory Robotic and Automation*, **8**(1), pp. 17–24.
- [17] Wang, J., and Gosselin, C. M., 2004, "Kinematic Analysis and Design of Kinematically Redundant Parallel Mechanisms," *ASME J. Mech. Des.*, **126**(1), pp. 109–118.
- [18] Ebrahimi, I., Carretero, J. A., and Boudreau, R., 2007, "3-PRRR Redundant Planar Parallel Manipulator: Inverse Displacement, Workspace and Singularity Analyses," *Mech. Mach. Theory*, **42**(8), pp. 1007–1016.
- [19] Hassan, M., and Notash, L., 2004, "Analysis of Active Joint Failure in Parallel Robot Manipulators," *ASME J. Mech. Des.*, **126**(6), pp. 959–968.
- [20] Kauschke, M., 1996, "Closed Form Solutions Applied to Redundant Serial

- Link Manipulators,” *Math. Comput. Simul.*, **41**, pp. 509–516.
- [21] Nakamura, Y., 1991, *Advanced Robotics: Redundancy and Optimization*, Addison-Wesley, Reading, MA.
- [22] Cha, S.-H., Lasky, T. A., and Velinsky, S. A., 2006, “Kinematic Redundancy Resolution for Serial-Parallel Manipulators via Local Optimization Including Joint Constraints,” *Mech. Based Des. Struct. Mach.*, **34**(2), pp. 213–239.
- [23] Gosselin, C. M., and Angeles, J., 1988, “The Optimum Kinematic Design of a Planar Three-Degree-of-Freedom Parallel Manipulator,” *ASME J. Mech., Transm., Autom. Des.*, **110**(1), pp. 35–41.
- [24] Ebrahimi, I., Carretero, J. A., and Boudreau, R., 2007, “Path Planning for the 3-PRRR Redundant Planar Parallel Manipulator,” *Proceedings of the 2007 IFToMM World Congress*.
- [25] Merlet, J.-P., 2006, *Parallel Robots*, 2nd ed., Springer, New York.
- [26] Merlet, J.-P., Gosselin, C. M., and Mouly, N., 1998, “Workspaces of Planar Parallel Manipulators,” *Mech. Mach. Theory*, **33**(1), pp. 7–20.
- [27] Gosselin, C. M., and Angeles, J., 1990, “Singularity Analysis of Closed-Loop Kinematic Chains,” *IEEE Trans. Rob. Autom.*, **6**(3), pp. 281–290.
- [28] Firmani, F., and Podhorodeski, R. P., 2005, “Force-Unconstrained Poses of the 3-PRR and 4-PRR Planar Parallel Manipulators,” *Trans. Can. Soc. Mech. Eng.*, **29**(4), pp. 617–628.